into the Rh-CH_3 bond probably occurs through the reaction of a geminate radical pair[20] that is trapped in the benzene solvent cage.

Conclusion

The physical properties and reactivity patterns of the Rh(TPP) species Rh(TPP)(H), $Rh(TPP)^-$, and $(Rh(TPP))_2$ are shown to be closely analogous to those of the more fully characterized Rh(OEP) species. Reactions of Rh(TPP)(H) with CO and H_2CO to produce the metalloformyl (Rh(TPP)(CHO)) and the hydroxymethyl ($Rh(TPP)(CH_2OH)$) complexes, respectively, are particularly important parallels with the reported Rh(OEP) system. The similarity in reactivity patterns for these electronically extreme types of porphyrin ligands (TPP, OEP) indicates that changing the electronic properties by substituent effects results in only minor changes at the rhodium center. We believe that the unusual organometallic chemistry presently observed only for rhodium porphyrins should occur for many sets of strong σ-donor ligands that produce planar low-spin rhodium(III) complexes.

Acknowledgment. This research was supported by the National Science Foundation and the Office of Basic Energy Sciences, DOE Grant No. DE-AC02-84ER-13133.

Registry No. $(TPP)[Rh(CO)_2]_2$, 88083-36-7; Rh(TPP)(I), 69509-35-9; Rh(TTP)(I), 103533-53-5; Rh(TPP)(H), 103533-54-6; Rh(TTP)(H), 103562-44-3; $Rh(TPP)^-$, 103533-55-7; $Rh(TTP)^-$, 103533-56-8; $[Rh(TPP)]_2$, 88083-37-8; $[Rh(TTP)]_2$, 103533-57-9; Rh(TPP)(CHO), 86412-76-2; Rh(TTP)(CHO), 86399-35-1; $Rh(TPP)(CH_3)$, 103562-25-0; $Rh(TPP)(C_2H_5)$, 103533-58-0; $Rh(TPP)(CH_2I)$, 69509-26-8; $[Rh(TPP)]_2(C_2H_4)$, 103533-59-1; $Rh(TTP)(CH_2OH)$, 103562-26-1; $Rh(TTP)[C(O)CH_3]$, 103533-60-4; $Rh(TTP)(CH_3)$, 103533-61-5; 1,2-dibromoethane, 106-93-4; formaldehyde, 50-00-0.

(20) Sweany, R. L.; Halpern, J. *J. Am. Chem. Soc.* **1977**, *99*, 8335.

Contribution from the Chemistry Department, The University of North Carolina, Chapel Hill, North Carolina 27514

Redox Properties of Polypyridyl-Aqua Complexes of Osmium

David W. Pipes and Thomas J. Meyer*

Received February 27, 1986

The electrochemical properties of the *trans*-dioxoosmium(VI) complexes $[(trpy)Os(O)_2(OH)]^+$ and $[(phen)Os(O)_2(OH)_2]$ (trpy = 2,2':6'2''-terpyridine and phen = 1,10-phenanthroline) have been studied in aqueous solutions over the pH range 0-14. Multiple electron, proton coupled redox steps are observed with the formation of lower oxidation state Os(III) and Os(II) hydroxo or aqua complexes upon reduction. Acid dissociation constants for aqua and hydroxo complexes and pH-dependent potential values for the redox couples that appear between Os(VI) and Os(II) were determined from pH-dependent electrochemical data. From the data available here and from data in earlier studies, variations in K_a values and redox potentials as pyridyl groups are replaced by aqua groups are discussed as to the role of the oxo group in stabilizing higher oxidation states.

There is an extensive, still emerging polypyridyl-oxo chemistry of Ru and Os based on the higher oxidation states VI, V, and IV.[1-6] Examples include $[(bpy)_2(py)Ru^{IV}{=}O]^{2+}$ (bpy = 2,2'-bipyridine; py = pyridine),[1] $[(trpy)Os^{VI}(O)_2(OH)]^+$ (trpy = 2,2':6',2''-terpyridine),[3] and *cis*- and *trans*-$[(bpy)_2M^{VI}(O)_2]^{2+}$ (M = Ru, Os).[4,5] A key to the formation of the high oxidation state complexes is the loss of protons and stabilization by electron donation from bound hydroxo or oxo groups. The accessibility of the higher oxidation states and the existence of a series of oxidation states within a narrow potential range enable the oxo complexes to act as effective stoichiometric and/or catalytic oxidants toward a variety of inorganic and organic substrates.[7-10]

The results of electrochemical studies on polypyridyl aqua-oxo complexes of Os, $[(trpy)(bpy)Os^{II}(OH_2)]^{2+}$[2] and *cis*- and *trans*-$[(bpy)_2Os^{VI}(O)_2]^{2+}$, have been reported.[4] We have extended that work to include a series of mixed aqua-oxo, polypyridyl complexes of Os and report here the results of the study and of the systematic variations in redox and acid-base properties that occur through the series.

Experimental Section

Materials. OsO_4 (>99%), 1,10 phenanthroline (gold label), and deuterium-labeled water were obtained from Aldrich Chemical Co. 2,2':6',2''-Terpyridine was obtained from G. F. Smith, Inc. Water was distilled over $KMnO_4$ before use. All other chemicals were reagent grade and used without further purification.

Measurements. Routine UV-vis spectra were obtained on a Bausch & Lomb 210 UV-vis 2000 spectrophotometer in 1-cm quartz cells. Spectroelectrochemical experiments were carried out in a three-compartment cell, where the working-electrode compartment was a quartz cell. Infrared spectra were obtained as KBr pellets on a Nicolet 20DX FTIR spectrometer. Proton NMR spectra were obtained in D_2O on a Bruker 250-MHz NMR spectrometer. Cyclic voltammetric experiments

(1) (a) Moyer, B.; Meyer, T. J. *Inorg. Chem.* **1981**, *20*, 436. (b) Moyer, B.; Meyer, T. J. *J. Am. Chem. Soc.* **1978**, *100*, 3601. (c) Yukawa, Y.; Aoyagi, K.; Kurihara, M.; Shirai, K.; Shimizu, K.; Mukaida, M.; Takeuchi, T.; Kakihana, H. *Chem. Lett.* **1985**, 283. (d) Marmion, M. E.; Takeuchi, K. J. *J. Am. Chem. Soc.* **1986**, *108*, 510. (e) Che, C.-M.; Wong, K.-Y.; Mak, T. C. W. *J. Chem. Soc., Chem. Commun.* **1985**, 546.

(2) (a) Takeuchi, K. J.; Thompson, M.; Pipes, D. W.; Meyer, T. J. *Inorg. Chem.* **1984**, *23*, 1845. (b) Roecker, L.; Kutner, W.; Gilbert, J. A.; Simmons, M.; Murray, R. W.; Meyer, T. J. *Inorg. Chem.* **1985**, *24*, 3784.

(3) Pipes, D. W.; Meyer, T. J. *J. Am. Chem. Soc.* **1984**, *106*, 7653.

(4) (a) Dobson, J. C.; Takeuchi, K. J.; Pipes, D. W.; Geselowitz, D. A.; Meyer, T. J. *Inorg. Chem.* **1986**, *25*, 2357. (b) Takeuchi, K. J.; Samuels, G. J.; Gersten, S. W.; Gilbert, J. A.; Meyer, T. J. *Inorg. Chem.* **1983**, *22*, 1407. (c) Che, C.-M.; Tang, T.-W.; Poon, C.-K. *Chem. Soc., J. Chem. Commun.* **1984**, 641.

(5) (a) Gilbert, J. A.; Eggleston, D. S.; Murphy, W. R., Jr.; Geselowitz, D. A.; Gersten, S. W.; Hodgson, D. J.; Meyer, T. J. *J. Am. Chem. Soc.* **1985**, *107*, 3855. (b) Che, C.-M.; Wong, K.-Y.; Leung, W.-H.; Poon, C.-K. *Inorg. Chem.* **1986**, *25*, 345.

(6) (a) Nikol'skii, A. B.; D'yachenko, Yu. I.; Myund, L. A. *Russ. J. Inorg. Chem. Engl. Transl.*) **1974**, *19*, 1368. (b) Griffith, W. P. *Coord. Chem. Rev.* **1972**, *8*, 369.

(7) (a) Moyer, B.; Meyer, T. J. *J. Am. Chem. Soc.* **1979**, *101*, 1326. (b) Ellis, C. D.; Gilbert, J. A.; Murphy, W. R., Jr.; Meyer, T. J. *J. Am. Chem. Soc.* **1983**, *105*, 4842. (c) Gilbert, J. A.; Gersten, S. W.; Meyer, T. J. *J. Am. Chem. Soc.* **1982**, *104*, 6872. (d) Vining, W. J.; Meyer, T. J. *J. Electroanal. Chem. Interfacial Electrochem.* **1985**, *195*, 183.

(8) (a) Thompson, M. S.; DeGiovani, W. F.; Moyer, B. A.; Meyer, T. J. *J. Org. Chem.* **1984**, *25*, 4972. (b) Moyer, B. A.; Thompson, M. S.; Meyer, T. J. *J. Am. Chem. Soc.* **1980**, *102*, 2310. (c) McHatton, R. C.; Anson, F. C. *Inorg. Chem.* **1984**, *23*, 3936.

(9) (a) Thompson, M. S.; Meyer, T. J. *J. Am. Chem. Soc.* **1982**, *104*, 4106. (b) Thompson, M. S.; Meyer, T. J. *J. Am. Chem. Soc.* **1982**, *104*, 5070. (c) Moyer, B. A.; Sipe, B. K.; Meyer, T. J. *Inorg. Chem.* **1981**, *20*, 1475. (d) Roecker, L.; Meyer, T. J. *J. Am. Chem. Soc.* **1986**, *108*, 4066. (e) Dobson, J. C.; Seok, W. K.; Meyer, T. J. *Inorg. Chem.* **1986**, *25*, 1514.

(10) Meyer, T. J. *J. Electrochem. Soc.* **1984**, *131*, 7, 221C.

0020-1669/86/1325-4042$01.50/0

Table I. ν(Os=O) Stretching Frequencies for Os(VI)–Dioxo Complexes

complex	$\nu_{asym}(Os(O)_2)$, cm^{-1}	$\nu_{sym}(Os(O)_2)$, cm^{-1} [a]
$[(trpy)Os(O)_2(OH)]NO_3$	845[a]	
$[(phen)Os(O)_2(OH)_2]$	825[b]	
trans-$[(bpy)_2Os(O)_2](ClO_4)_2$	872[c]	
cis-$[(bpy)_2Os(O)_2](ClO_4)_2$	833[c]	863[c]
$[(py)_2(O_2C_2H_4)Os(O)_2]$	833[d]	
$[(bpy)Os(O)_2]_2(O)_2$	828[e]	868[e]
$[(py)_2Os(O)_2]_2(O)_2$	842[e]	874[e]

[a] KBr pellet. [b] References 15 and 16. [c] Reference 4. [d] Reference 6a. [e] Reference 6b.

were obtained in one-compartment cells using either a Tokai[11] glassy-carbon electrode or a hanging-mercury-drop electrode (HMDE) as the working electrode, a Pt wire as the auxilary electrode, and either a saturated sodium calomel (SSCE) or a Ag/AgCl reference electrode. Cyclic voltammograms were obtained on a PAR 173 galvanostat/potentiostat connected to a Super Cyclic wave generator[12] or a PAR 175 universal programer. Coulometric studies were carried out in two- or three-compartment cells using either a reticulated vitreous-carbon[13] electrode or a mercury pool as the working electrode. Potentials were applied by using a PAR 173 galvanostat/potentiostat, and electrical equivalents were measured with a PAR 179 digital coulometer. In several pH regions the electrode processes are considerably irreversible electrochemically, and measurements at C electrodes were aided by using oxidatively activated electrodes and an activation procedure described earlier.[14]

Preparations. Literature procedures were used to prepare the complexes $K_2[Os^{VI}(O)(OH)_4]$[15] and $(phen)Os^{VI}(O)_2(OH)_2$.[16,17] The crystal structure of the dioxo complex has been reported and verifies the *trans*-dioxo geometry at Os with Os–O bond lengths of 1.742 Å.[16]

$[(trpy)Os(O)_2(OH)]NO_3 \cdot 2H_2O$. To 0.165 g of $K_2[Os(O)_2(OH)_4]$ dissolved in 20 mL of water was added dropwise 20 mL of an aqueous solution of 1 equiv of trpy dissolved by the addition of ~3 mL of 0.1 M H_2SO_4. The pH of the solution was maintained at <8 by the addition of 0.1 M H_2SO_4 as needed. The solution was stirred for 30 min and filtered. An aqueous saturated solution of $NaNO_3$ (1 mL) was added dropwise to the filtrate and the solution allowed to stand for 24 h. Thin brown, diamond-shaped plates mixed with a brown powder formed. The product was filtered, washed three times with H_2O, and dried under vacuum. Anal. Calcd: C, 31.57; H, 2.66; N, 9.82. Found: C, 31.55; H, 2.83; N, 9.78.

Determination of the Acid Dissociation Constant for $[(trpy)Os(O)(OH)(OH_2)]^{3+}$. The acid dissociation constant for $[(trpy)Os^{VI}(O)(OH)(OH_2)]^{3+}$ to give $[(trpy)Os(O)_2(OH)]^+$ was determined spectrophotometrically in aqueous solutions at 23.0 (±0.2) °C at μ = 1.0 M in $NaClO_4$. Aliquots of $[(trpy)Os(O)_2(OH)]^+$ were added to 10-mL volumetric flasks to give final Os concentrations of 6.99×10^{-5} M, and the pH was adjusted by the addition of 0.2 M $HClO_4$. The final ionic strength of μ = 1.0 M was achieved by the addition of $NaClO_4$. The concentrations of acid and base in the equilibrium were determined spectrophotometrically by using λ_{max} = 377 nm ($\epsilon = 9.0 \times 10^3$ M^{-1} cm^{-1}) for $[(trpy)Os(O)(OH)(OH_2)]^{3+}$ and λ_{max} = 350 nm ($\epsilon = 1.0 \times 10^4$ M^{-1} cm^{-1}) for $[(trpy)Os(O)_2(OH_2)]^{2+}$.

Results

Infrared and ^1H NMR Spectra. For the *trans*-dioxo complexes of Os(VI) the single, asymmetric stretch of the *trans*-dioxo group is observed between 800 and 900 cm^{-1} (Table I). The symmetric stretch, which is forbidden in the *trans*-dioxo structure, is observed at higher energies in the cis complexes and has also been observed in cases where the *trans*-dioxo group is not strictly linear.

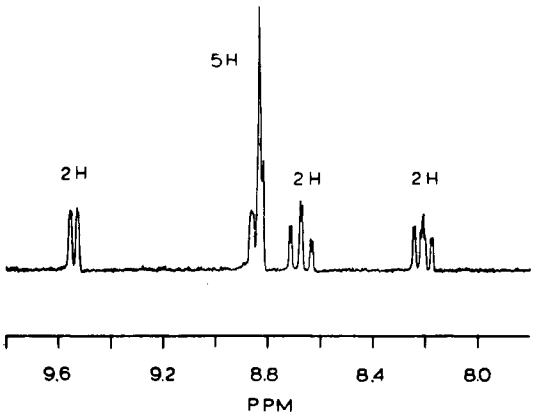

Figure 1. ^1H NMR spectrum of $[(trpy)Os^{VI}(O)_2(OH)]^+$ in D_2O vs. external Me_4Si.

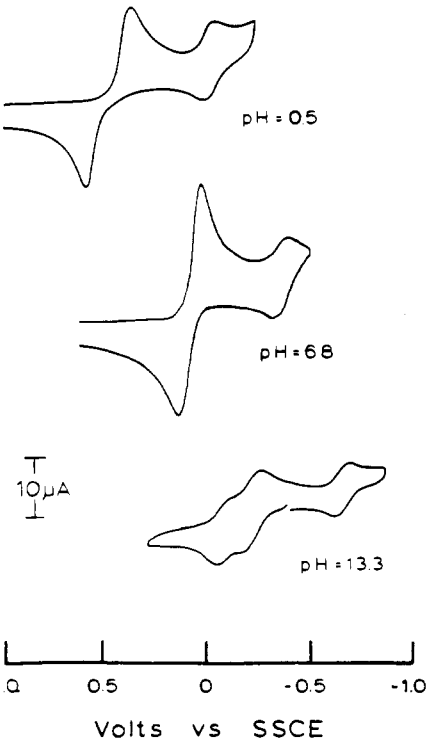

Figure 2. Cyclic voltammograms of ~0.1 mM aqueous solutions of $[(trpy)Os^{VI}(O)_2(OH)]^+$ at various pH values with glassy-carbon working electrodes vs. SSCE at 100 mV/s sweep rates.

An ^1H NMR spectrum of $[(trpy)Os^{VI}(O)_2(OH)]^+$ in D_2O is shown in Figure 1. The spectrum is typical for diamagnetic, polypyridyl complexes of Os(VI),[4,18] with the terpyridine hydrogens in the range 7.5–10 ppm showing the expected pattern for a single plane of symmetry splitting the terpyridine into equivalent halves. The spectrum can be described as two triplets at 8.20 and 8.66 ppm, each integrating to two hydrogens, a sharp multiplet at 8.84 ppm integrating to give hydrogens, and a doublet at 9.55 ppm integrating to two hydrogens.

Electrochemistry. The aqueous electrochemistries of $[(trpy)Os(O)_2(OH)]^+$ and $[(phen)Os(O)_2(OH)_2]$ were studied over the pH range $0 < pH < 14$. Cyclic voltammograms in solutions of pH ~0.5, 7, and 13 are shown in Figures 2 and 3. The $E_{1/2}$ values for the various couples observed are shown plotted as a function of pH in Figures 4 and 5. In the resulting Pourbaix diagrams, the dominant oxidation states of the metal in the various pH–potential regions are shown at the right. The proton compositions of the complexes in the various pH regions are represented by the

(11) Tokai carbon was obtained from Tokai Chemical Co., Tokyo, Japan.
(12) Woodward, W. S.; Rocklin, R. D.; Murray, R. W. *Chem. Biomed. Environ. Instrum.* **1979**, *9*, 95.
(13) Reticulated vitreous carbon was obtained from Chemotronics International, Inc., Ann Arbor, MI 48104.
(14) Cabaniss, G. E.; Diamantis, A. A.; Murphy, W. R., Jr.; Linton, R. W.; Meyer, T. J. *J. Am. Chem. Soc.* **1985**, *107*, 1847.
(15) Lott, K. A. K.; Symons, M. C. R. *J. Chem. Soc.* **1960**, *973*.
(16) Chang, C.-H.; Midden, W. R.; Deetz, J. S.; Behrman, E. J. *Inorg. Chem.* **1979**, *18*, 1364.
(17) Galas, A. M. R.; Hursthouse, M. B.; Behrman, E. J.; Midden, W. R.; Green, G.; Griffith, W. P. *Transition Met. Chem. (Weinheim, Ger.)* **1981**, *6*, 194.
(18) Pipes, D. W., Ph.D. Dissertation, University of North Carolina at Chapel Hill, 1985.

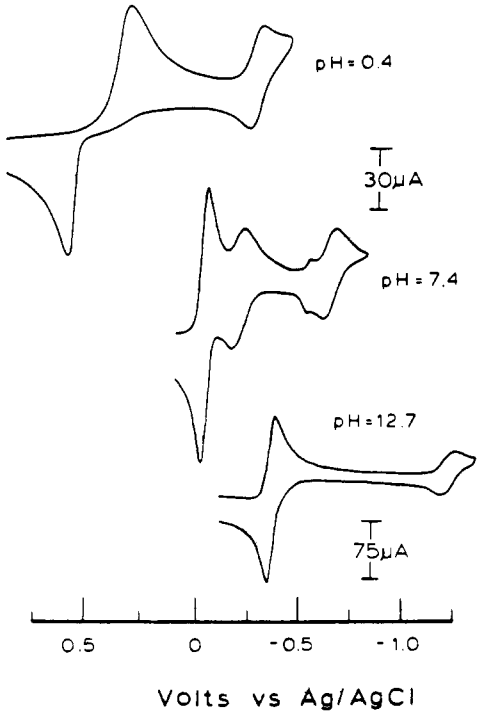

Figure 3. Cyclic voltammograms of ~0.1 mM aqueous solutions of $[(phen)Os^{VI}(O)_2(OH)_2]$ with a glassy-carbon working electrode (pH 0.40) and hanging-mercury-drop electrode HMDE (pH 7.4 and 12.7) vs. the Ag/AgCl reference electrode at sweep rates of 100 mV/s.

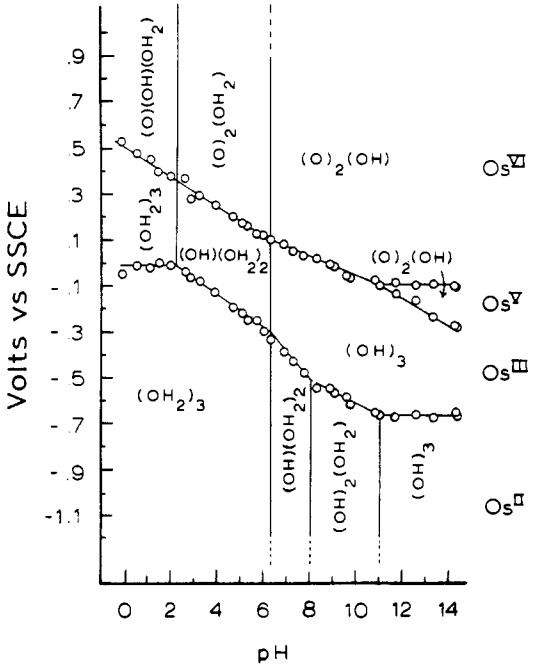

Figure 4. Pourbaix diagram ($E_{1/2}$ vs. pH profile) for $[(trpy)Os^{VI}(O)_2(OH)]^+$ in aqueous solutions (μ = 0.1 M) with glassy-carbon working electrodes vs. SSCE. See text for definition of symbols and description of data.

symbols showing the aqua, hydroxo, and oxo ligands. For example, for $[(trpy)Os^{VI}(O)_2(OH)]^+$ in the pH range 6.6 < pH < 8.0 the symbols used for oxidation states VI, III, and II are $Os^{VI}(O)_2(OH)$, $Os^{III}(OH)_3$, and $Os^{II}(OH)(OH_2)_2$, which refer to $[(trpy)Os^{VI}(O)_2(OH)]^+$, $[(trpy)Os^{III}(OH)_3]$, and $[(trpy)Os^{II}(OH)(OH_2)_2]^+$. The proton compositions of the complexes were determined by comparing the slopes of the $E_{1/2}$ vs. pH lines to values calculated from the Nernst equation: $E_{1/2} = E_{1/2}° - (0.059m/n)$pH, where $E_{1/2}°$ is the half-wave potential at pH 0 and m is the number of protons gained when n electrons are gained. For example, a slope

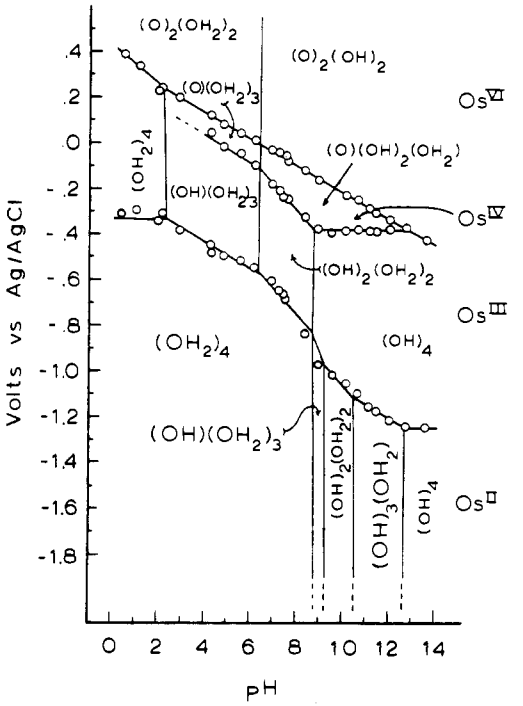

Figure 5. Pourbaix diagram ($E_{1/2}$ vs. pH profile) of $[(phen)Os^{VI}(O)_2(OH)_2]$ in aqueous solutions with glassy carbon working electrodes (pH <4) and HMDE (pH <4) vs. the Ag/AgCl reference electrode. See text for definition of symbols and description of data.

of −59 mV/pH unit indicates a proton to electron ratio of 1:1, appropriate to processes involving H^+:e^- ratios of $1H^+$:$1e^-$, $2H^+$:$2e^-$, $3H^+$:$3e^-$, etc. For a slope of −118 mV/pH unit, the proton to electron ratio is 2:1: $2H^+$:$1e^-$, $4H^+$:$2e^-$, etc. Other ratios found here are −30 mV/pH unit ($1H^+$:$2e^-$), −39 mV/pH unit ($2H^+$:$3e^-$), −89 mV/pH unit ($3H^+$:$2e^-$), and 0 mV/pH unit ($0H^+$:ne^-). Note that the Nernst equation is strictly applicable only for electrochemically reversible couples. Deviations of measured slopes from those calculated from the Nernst equation can appear for quasi-reversible or irreversible processes since the wave shapes for such processes are determined, at least in part, by the kinetics of the heterogeneous charge-transfer process.

$[(trpy)Os^{VI}(O)_2(OH)]^+$. For the waves appearing in cyclic voltammograms of $[(trpy)Os(O)_2(OH)]^+$ at pH 0.5 and 6.8 (Figure 2), coulometric studies show that the more oxidative wave involves three electrons (n = 3.0 ± 0.2) and an Os(VI)/Os(III) couple and the second wave one electron (n = 1.0 ± 0.1) and an Os(III)/Os(II) couple. Further evidence for the numbers of electrons involved in the Os(VI)/Os(III) and Os(III)/Os(II) couples was obtained by rotating-disk experiments where the limiting-current ratio for the two waves was observed to be 3:1. Cyclic voltammetric (Figure 2) and coulometric studies at pH 13.3 show that the three-electron process has split into a one-electron (n = 1.0 ± 0.2) Os(VI)/Os(V) couple and a two-electron (n = 2.0 ± 0.2) Os(V)/Os(III) couple. The Os(III)/Os(II) couple remains one electron in character (n = 1.0 ± 0.1).

The Pourbaix diagram for $[(trpy)Os^{VI}(O)_2(OH)]^+$ can be interpreted in terms of the acid–base properties of the various oxidation states: From $0 < pH < 2.2$, the potential of the Os(VI)/Os(III) couple varies with pH with a slope of −59 mV/pH unit while the Os(III)/Os(II) couple is pH-independent. In this pH region the two couples are

$$[(trpy)Os^{VI}(O)(OH)(OH_2)]^{3+} + 3e^- + 3H^+ \rightarrow [(trpy)Os^{III}(OH_2)_3]^{3+}$$

$$[(trpy)Os^{III}(OH_2)_3]^{3+} + e^- \rightarrow [(trpy)Os^{II}(OH_2)_3]^{2+}$$

This interpretation of the pH dependence of the electrochemistry demands that protonation of one of the oxo groups in Os(VI) occurs at pH <2.2. Such a conclusion is supported by the pH

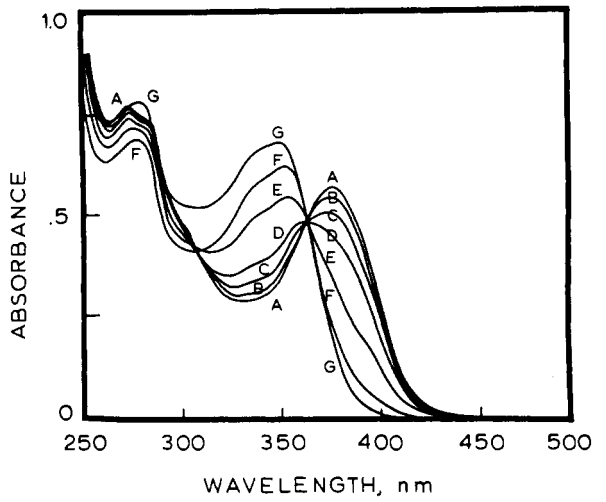

Figure 6. Electronic spectra (1-cm path length) of solutions 6.99×10^{-5} M in $[(trpy)Os^{VI}(O)_2(OH)]^+$ at $\mu = 1.0$ M in $NaClO_4$ at pH (A) 0.91, (B) 1.68, (C) 2.14, (D) 2.50, (E) 3.06, (F) 3.66, and (G) 7.22.

dependence of the electronic spectrum of Os(VI) in this pH region. In Figure 6 are shown electronic spectra for the Os(VI) complex over the pH range $0.91 < pH < 3.66$. The well-defined isosbestic point at $\lambda = 373$ nm is notable. On the basis of $\lambda_{max} = 377$ nm ($\epsilon = 9.0 \times 10^3$ M^{-1} cm^{-1}, for $[(trpy)Os(O)(OH)(OH_2)]^{3+}$ and $\lambda_{max} = 350$ nm ($\epsilon = 1.0 \times 10^4$ M^{-1} cm^{-1}) for $[(trpy)Os(O)_2(OH_2)]^{2+}$, $K_a = 3.4 \times 10^{-3}$ M ($pK_a = 2.47 \pm 0.30$; from six measurements) for $[(trpy)Os(O)(OH)(OH_2)_2]^{3+}$, in reasonable agreement with $pK_a = 2.2$ determined from the pH-dependent electrochemical data in Figure 4. The electrochemical data show that the second pK_a occurs at 6.3 due to loss of a proton from the aqua ligand.

$$[(trpy)Os^{VI}(O)_2(OH_2)]^{2+} \rightleftharpoons [(trpy)Os^{VI}(O)_2(OH)]^+ + H^+ \quad (1)$$

The spectrum at pH 7.22 in Figure 6 is included to show the relatively subtle spectral differences between $[(trpy)Os(O)_2OH)_2]^{2+}$ (F) and $[(trpy)Os(O)_2(OH)]^+$ (G). Slight shifts occur from $\lambda_{max} = 350$ nm to $\lambda_{max} = 348$ nm and from $\lambda_{max} \sim 271$ nm to $\lambda_{max} \sim 275$ nm, and the intensities of both bands increase. The shoulder at $\lambda = 282$ nm for $[(trpy)Os(O)_2(OH_2)]^{2+}$ is also observed at pH >6.3.

In the pH range $2.2 < pH < 6.3$, the potential of the Os(III)/Os(II) couple decreases by −59 mV/pH unit, indicating that the couple is $[(trpy)Os^{III}(OH)(OH_2)_2]^{2+}/[(trpy)Os^{II}(OH_2)_3]^{2+}$. From the electrochemical data, as verified by spectral changes, $pK_{a,1} = 2.2$ for the Os(III) complex:

$$[(trpy)Os^{III}(OH_2)_3]^{3+} \rightleftharpoons [(trpy)Os^{III}(OH)(OH_2)_2]^{2+} + H^+$$

The slope of the $E_{1/2}$ vs. pH plot for the Os(VI)/Os(III) couple remains ~−59 mV/pH unit. Since $pK_{a,1}$ for Os(III) is reached at pH 2.2, a pK_a for Os(VI) must also occur in this region in agreement with the spectrally determined value of $pK_a = 2.47$ (±0.30) ($\mu = 1.0$ M). From $2.2 < pH < 6.3$, the two couples are

$$[(trpy)Os^{III}(OH)(OH_2)_2]^{2+} + e^- + H^+ \rightarrow [(trpy)Os^{II}(OH_2)_3]^{2+}$$

$$[(trpy)Os^{VI}(O)_2(OH_2)]^{2+} + 3e^- + 3H^+ \rightarrow [(trpy)Os^{III}(OH)(OH_2)_2]^{2+}$$

In the pH region $6.3 < pH < 11.0$, the slope of the Os(VI)/Os(III) couple becomes −40 mV/pH unit, indicating a $2H^+/3e^-$ couple. The slope for the Os(III)/Os(II) couple is −118 mV/pH unit from $6.3 < pH < 8.0$, indicating a $2H^+/1e^-$ couple. The data suggest that a pK_a value for Os(III) must be reached near pH 6.3, and examination of electronic spectral data for Os(VI), Os(III), and Os(II) at pH ≥6.8 suggests that pK_a values for all three oxidation states must occur near this pH. To make the Pourbaix diagram internally consistent, we are forced to conclude that near pH ~6.3 both $pK_{a,2}$ and $pK_{a,3}$ for Os(III) must be reached ($K_{a,2}K_{a,3} = 1 \times 10^{-12}$ M^{-2})

$$[(trpy)Os^{III}(OH)(OH_2)_2]^{2+} \rightleftharpoons [(trpy)Os^{III}(OH)_3] + 2H^+$$

as well as $pK_{a,1}$ for Os(II)

$$[(trpy)Os^{II}(OH_2)_3]^{2+} \rightleftharpoons [(trpy)Os^{II}(OH)(OH_2)_2]^+ + H^+$$

and the second proton loss from Os(VI) (eq 1).

The spectral data show no further changes in proton content for Os(III) at pH >6.8, and up to pH 8.0 the couples are

$$[(trpy)Os^{VI}(O)_2(OH)]^+ + 3e^- + 2H^+ \rightarrow [(trpy)Os^{III}(OH)_3]$$

$$[(trpy)Os^{III}(OH)_3] + e^- + 2H^+ \rightarrow [(trpy)Os^{II}(OH)(OH_2)_2]^+$$

The slope changes to −59 mV/pH unit at pH 8.0 for the Os(III)/Os(II) couple, and so $pK_{a,2}$ for $[(trpy)Os^{II}(OH_2)_3]^{2+}$ must occur at pH 8.0 and past pH = 8.0 the couple becomes

$$[(trpy)Os^{III}(OH)_3] + e^- + H_2O \rightarrow [(trpy)Os^{II}(OH)_2(OH_2)] + OH^-$$

At *pH >11.0* the three-electron Os(VI)/Os(III) couple separates into a pH-independent $1e^-$ Os(VI)/Os(V) couple and a $2H^+/2e^-$ Os(V)/Os(III) couple

$$[(trpy)Os^{VI}(O)_2(OH)]^+ + e^- \rightarrow [(trpy)Os^{V}(O)_2(OH)]$$

$$[(trpy)Os^{V}(O)_2(OH)] + 2e^- + 2H_2O \rightarrow [(trpy)Os^{III}(OH)_3] + 2OH^-$$

The loss of a pH dependence for the Os(III)/Os(II) couple past pH 11.0 suggests that $pK_{a,3}$ for Os(II) is reached at ~11.0 where the Os(III)/Os(II) couple becomes

$$[(trpy)Os^{III}(OH)_3] + e^- \rightarrow [(trpy)Os^{II}(OH)_3]^-$$

$[(phen)Os(O)_2(OH)_2]$. The aqueous electrochemistry of $[(phen)Os^{VI}(O)_2(OH)_2]$ is even more complex because of the additional hydroxo group and the fact that Os(VI) is a stable oxidation state in the range $4 < pH < 12.7$, but Os(V) is thermodynamically unstable over the complete pH range. Cyclic voltammograms for $[(phen)Os^{VI}(O)_2(OH)_2]$ at pH 0.4, 7.4, and 12.7 are shown in Figure 3. From coulometric studies the following results were obtained: (1) At pH 1.0 $n = 3.0$ (±0.3) for the Os(VI)/Os(III) couple and $n = 1.0$ (±0.2) for the Os(III)/Os(II) couple. (2) At pH 6.8 $n = 2.0$ (±0.2) for the Os(VI)/Os(IV) couple and $n = 1.0$ (±0.1) for the Os(IV)/Os(III) couple.

From *0 < pH < 2.4*, the Os(III)/Os(II) couple is pH-independent and the Os(VI)/Os(III) wave has a slope of −80 mV/pH unit, suggesting the couples

$$[(phen)Os^{III}(OH_2)_4]^{3+} + e^- \rightarrow [(phen)Os^{II}(OH_2)_4]^{2+}$$

$$[(phen)Os^{VI}(O)_2(OH_2)_2]^{2+} + 3e^- + 4H^+ \rightarrow [(phen)Os^{III}(OH_2)_4]^{3+}$$

At *2.4 < pH < 6.2* the Os(III)/Os(II) couple becomes a $1e^-/1H^+$ couple because $pK_{a,1} = 2.4$ is reached for Os(III), the slope for the Os(VI)/Os(III) couple increases to −60 mV/pH unit over the pH range $2.4 < pH < 4.0$, and the couples appear to be

$$[(phen)Os^{III}(OH)(OH_2)_3]^{2+} + e^- + H^+ \rightarrow [(phen)Os^{II}(OH_2)_4]^{2+}$$

$$[(phen)Os^{VI}(O)_2(OH_2)_2]^{2+} + 3e^- + 3H^+ \rightarrow [(phen)Os^{III}(OH)(OH_2)_3]^{2+}$$

The use of the HMDE at pH >4.0 gave electrochemically more reversible behavior and clearly separated Os(IV)/Os(III) and Os(VI)/Os(IV) couples (Figure 3). The nature of the couples can be inferred from the slopes of the $E_{1/2}$ vs. pH plots and from the −60 mV/pH unit slopes in the range $4.0 < pH < 6.2$; the couples are

Table II. Electronic Spectra in Water at Various pH Values (μ = 1.0 M)

I. $[(trpy)Os(O)_2(OH)]NO_3$

pH	complex[a]	λ, nm (ε, M^{-1} cm^{-1})	pH	complex[a]	λ, nm (ε, M^{-1} cm^{-1})
1.0	$[(trpy)Os^{VI}(O)(OH)(OH_2)]^{3+}$	377 (9.0×10^3)	6.8	$[(trpy)Os^{II}(OH)(OH_2)_2]^{+}$[c]	661 (2.6×10^3)
		282 sh			603 sh
		271 (1.0×10^4)			538 sh
	$[(trpy)Os^{III}(OH_2)_3]^{3+}$	525 sh			456 (4.3×10^3)
		465 sh			369 sh
		417 (1.8×10^3)			321 (2.3×10^4)
		324 sh			276 (2.0×10^4)
		307 sh	11.4	$[(trpy)Os^{VI}(O)_2(OH)]^{+}$	348 (1.1×10^4)
		270 (1.9×10^4)			276 (1.2×10^4)
	$[(trpy)Os^{II}(OH_2)_3]^{2+}$	660 (2.5×10^3)		$[(trpy)Os^{III}(OH)_3]$	658 sh
		603 sh			549 (2.2×10^3)
		539 (2.8×10^3)			409 (3.3×10^3)
		447 (4.0×10^3)			309 (1.6×10^4)
		369 sh			275 (2.1×10^4)
		320 (2.5×10^4)		$[(trpy)Os^{II}(OH)_3]^{-}$	754 sh
		275 (1.9×10^4)			638 (2.6×10^3)
3.5	$[(trpy)Os^{VI}(O)_2(OH_2)]^{2+}$	350 (1.0×10^4)			506 (4.4×10^3)
		271 (1.1×10^4)			406 (5.5×10^3)
	$[(trpy)Os^{III}(OH_2)_2(OH)]^{2+}$	681 sh			309 sh
		564 sh			277 (2.0×10^4)
		515 sh	12.6	$[(trpy)Os^{VI}(O)_2(OH)]^{+}$	348 (1.2×10^4)
		478 sh			277 (1.3×10^4)
		451 (2.6×10^3)		$[(trpy)Os^{V}(O)_2(OH)]$	642 sh
		392 (2.5×10^3)			556 (2.0×10^3)
		313 (1.8×10^4)			395 sh (3.3×10^3)
		272 (2.1×10^4)		$[(trpy)Os^{III}(OH)_3]$	668 sh
	$[(trpy)Os^{II}(OH_2)_3]^{2+}$	660 (2.5×10^3)			547 (2.2×10^3)
		603 sh			408 (3.3×10^3)
		539 (2.8×10^3)			316 (1.7×10^4)
		449 (4.0×10^3)			276 (2.1×10^4)
		369 sh		$[(trpy)Os^{II}(OH)_3]^{-}$	655 (2.3×10^3)
		320 (2.5×10^4)			519 (4.4×10^3)
		275 (1.9×10^4)			412 (5.5×10^3)
6.8	$[(trpy)Os^{VI}(O)_2(OH)]^{+}$	450 (1.2×10^4)			318 (1.6×10^4)
		348			278 (1.8×10^4)
		275 (1.25×10^4)			
	$[(trpy)Os^{III}(OH)_3]$[b]	613 sh			
		514 (2.3×10^2)			
		400 (3.4×10^2)			
		317 (1.8×10^4)			
		275 (2.1×10^4)			

II. $[(phen)Os^{VI}(O)_2(OH)_2]$

pH	complex	λ, nm (ε, M^{-1} cm^{-1})	pH	complex	λ, nm (ε, M^{-1} cm^{-1})
1.0	$[(phen)Os^{VI}(O)_2(OH_2)_2]^{2+}$		6.8	$[(phen)Os^{IV}(O)(OH)_2(OH_2)]$	450 sh
	$[(phen)Os^{III}(OH_2)_4]^{3+}$	538 sh			361 (5.1×10^3)
		447 sh		$[(phen)Os^{III}(OH)_2(OH_2)_2]^{+}$	556 sh
		377 (6.4×10^3)			457 (5.4×10^3)
		361 sh			387 (4.0×10^3)
	$[(phen)Os^{II}(OH_2)_4]^{2+}$	692 (2.2×10^3)			365 (5.2×10^3)
		528 sh		$[(phen)Os^{II}(OH_2)_4]^{2+}$	694 (2.3×10^3)
		478 (8.0×10^3)			500 sh
		413 sh			484 (8.0×10^3)
		330 sh			420 sh
4.3	$[(phen)Os^{VI}(O)_2(OH_2)_2]^{2+}$				330 sh
	$[(phen)Os^{III}(OH)(OH_2)_3]^{2+}$	499 sh	10.5	$[(phen)Os^{VI}(O)_2(OH)_2]$	430 (1.0×10^2)
		421 (4.1×10^3)			345 (8.0×10^2)
		384 (4.4×10^3)		$[(phen)Os^{IV}(O)(OH)_2(OH_2)]$	450 sh
		367 (4.5×10^3)			361 (5.0×10^2)
	$[(phen)Os^{II}(OH_2)_4]^{2+}$	691 (2.3×10^3)		$[(phen)Os^{III}(OH)_4]^{-}$	660 sh
		528 sh			514 (7.0×10^2)
		480 (8.0×10^3)			470 sh
		421 sh			385 sh
		330 sh			348 sh
6.8	$[(phen)Os^{VI}(O)_2(OH)_2]$[d]	430 (1.3×10^2)			333 sh
		347 (8.7×10^2)		$[(phen)Os^{II}(OH)_3(OH_2)]^{-}$[e]	580 sh
		296 sh (1.7×10^3)			493 (8.0×10^2)
		272 (2.83×10^4)			440 sh
		223 (3.23×10^4)			393 sh

[a] The spectra of complexes of oxidation states V–II were generated electrochemically. [b] Both $[(trpy)Os^{III}(OH)_2(OH_2)]^{+}$ and $[(trpy)Os^{III}(OH)_3]$ are present. [c] The spectrum is of a mixture of $[(trpy)Os^{II}(OH)(OH_2)_2]^{+}$ and $[(trpy)Os^{II}(OH_2)_3]^{2+}$. [d] Reference 16. [e] Both $[(phen)Os^{II}(OH)_2(OH_2)_2]$ and $[(phen)Os^{II}(OH)_3(OH_2)]^{-}$ are present in the solution.

Table III. Thermodynamically Stable Oxidation States of Polypyridyl–Aqua Complexes of Os

starting complex	observable oxidn states[a] pH 1.0	pH 4.0	pH 13	reference
$[(trpy)(bpy)Os(OH_2)]^{2+}$	V–II	V–II	IV, II, (V)[b]	2a
cis-$[(bpy)_2Os^{VI}(O)_2]^{2+}$	VI, V, III, II	VI–II	VI, V, III, II	4a
trans-$[(bpy)_2Os^{VI}(O)_2]^{2+}$	VI, III, II	VI, III, II	VI, V, III, II	4a
$[(trpy)Os^{VI}(O)_2(OH)]^{+}$	VI, III, II	VI, III, II	VI, V, III, II	this work
$[(phen)Os^{VI}(O)_2(OH)_2]$	VI, III, II	VI, IV–II	VI, III, II	this work

[a] By cyclic voltammetry, spectral observations, and in some cases, chemical isolation. [b] The Os(V)/Os(IV) couple is beyond the oxidative solvent limit.

$$[(phen)Os^{VI}(O)_2(OH_2)_2]^{2+} + 2e^- + 2H^+ \rightarrow [(phen)Os^{IV}(O)(OH_2)_3]^{2+}$$

$$[(phen)Os^{IV}(O)(OH_2)_3]^{2+} + e^- + H^+ \rightarrow [(phen)Os^{III}(OH)(OH_2)_3]^{2+}$$

Given the characteristic appearance of the monooxo group in complexes of Ru(IV) and Os(IV), it is most likely that the Os(IV) complex is the oxo ion $[(phen)Os^{IV}(O)(OH_2)_3]^{2+}$, although in terms of proton content it could equally well be written as $[(phen)Os^{IV}(OH)_2(OH_2)_2]^{2+}$.

From $6.2 < pH < 8.7$ the slope of the Os(III)/Os(II) couple is −120 mV/pH unit, indicating that a second pK_a for Os(III) is reached at pH 6.2. The slope of the Os(IV)/Os(III) couple also becomes −120 mV/pH unit. To be internally consistent, a pK_a value for Os(IV) must occur in the same region involving the loss of $2H^+$, and the couples are

$$[(phen)Os^{IV}(O)(OH)_2(OH_2)] + e^- + 2H^+ \rightarrow [(phen)Os^{III}(OH)_2(OH_2)_2]^{+}$$

$$[(phen)Os^{III}(OH)_2(OH_2)_2]^{+} + e^- + 2H^+ \rightarrow [(phen)Os^{II}(OH_2)_4]^{2+}$$

Spectroscopic studies are consistent with pK_a values for Os(IV) and Os(III) occurring in this region as shown by shifts in λ values toward longer wavelengths (Table II). The slope of the Os(VI)/Os(IV) couple remains −60 mV/pH unit, and so a K_a value for the Os(VI) complex must also be reached in this region that involves the loss of $2H^+$, and the couple is

$$[(phen)Os^{VI}(O)_2(OH)_2] + 2e^- + 2H^+ \rightarrow [(phen)Os^{IV}(O)(OH)_2(OH_2)]$$

From $8.7 < pH < 9.3$, the slope of the Os(III)/Os(II) couple decreases to −177 mV/pH unit, suggesting a $3e^-/1H^+$ couple. Because of slow charge-transfer kinetics, the $E_{1/2}$ vs. pH data in this region are not very accurate and the plot shown was drawn so that the data for the whole Pourbaix diagram are internally consistent. The pH independence of the Os(IV)/Os(III) couple at pH >8.7 suggests that a pK_a for Os(III) has been reached in which two protons are lost.

$$[(phen)Os^{III}(OH)_2(OH_2)_2]^{+} \rightleftharpoons [(phen)Os^{III}(OH)_4]^{-} + 2H^+$$

Spectroscopic evidence shows that a pK_a for the Os(II) complex must also exist at pH ~8.7. From this analysis, in the range $8.7 < pH < 9.3$, the three couples are

$$[(phen)Os^{VI}(O)_2(OH)_2] + 2e^- + 2H_2O \rightarrow [(phen)Os^{IV}(O)(OH)_2(OH_2)] + 2OH^-$$

$$[(phen)Os^{IV}(O)(OH)_2(OH_2)] + e^- \rightarrow [(phen)Os^{III}(OH)_4]^-$$

$$[(phen)Os^{III}(OH)_4]^- + e^- + 3H_2O \rightarrow [(phen)Os^{II}(OH)(OH_2)_3]^{+} + 3OH^-$$

where, once again, the ambiguities of several of the proton assignments should be noted.

Throughout the pH region $9.3 < pH < 12.7$, the Os(VI)/Os(IV) and Os(IV)/Os(III) couples are pH-independent. However, the slope of the Os(III)/Os(II) couple in the pH range $9.3 < pH < 10.5$ increases to −118 mV/pH unit, indicating the appearance of a pK_a for Os(II) and the couple

$$[(phen)Os^{III}(OH)_4]^- + e^- + 2H_2O \rightarrow [(phen)Os^{II}(OH)_2(OH_2)_2] + 2OH^-$$

The third pK_a for Os(II) is reached at pH 10.5, and the couple becomes

$$[(phen)Os^{III}(OH)_4]^- + e^- + H_2O \rightarrow [(phen)Os^{II}(OH)_3(OH_2)]^- + OH^-$$

Past $pH > 12.7$, the potential of the Os(IV)/Os(III) couple falls below the potential of the Os(VI)/Os(IV) couple to give a $3e^-/2H^+$ (−40 mV/pH unit) Os(VI)/Os(III) couple. Past pH >12.7 the Os(III)/Os(II) couple becomes independent of pH because of the loss of an additional proton from Os(II), and the two couples observed are

$$[(phen)Os^{VI}(O)_2(OH)_2] + 3e^- + 2H_2O \rightarrow [(phen)Os^{III}(OH)_4]^- + 2OH^-$$

$$[(phen)Os^{III}(OH)_4]^- + e^- \rightarrow [(phen)Os^{II}(OH)_4]^{2-}$$

Electronic Spectra. The absorption features that appear in the electronic spectrum of $[(trpy)Os^{VI}(O)_2(OH)]^+$ and $[(phen)Os^{VI}(O)_2(OH)_2]$ and their Os(V), Os(IV), Os(III), and Os(II) reduced forms, where available, are summarized in Table II at a series of pH values. The spectra of the Os complexes in lower oxidation states were obtained by electrochemical generation in spectroelectrochemical cells at potentials determined from the Pourbaix diagrams. Proton compositions were deduced from the Pourbaix diagrams in Figures 3 and 4. In general, the spectra are similar to those of other polypyridyl complexes[2a,4,6,16,19] in the

Table IV. pH-Independent Os(III)/Os(II) Reduction Potentials and Acid Dissociation Constants for Os(III) and Os(II)

couple[a,b]	Os(II) $E_{1/2}$[c]	$K_{a,1}$	$K_{a,2}$	$K_{a,3}$	$K_{a,4}$	Os(III) $K_{a,1}$	$K_{a,2}$	$K_{a,3}$
$[(trpy)(bpy)Os(OH_2)]^{3+/2+}$	0.41	1.6×10^{-8}				1.0×10^{-2}		
$[(trpy)(bpy)Os(OH)]^{2+/+}$	0.08							
cis-$[(bpy)_2Os(OH_2)_2]^{3+/2+}$	0.16	1.3×10^{-8}	1.0×10^{-11}			1.3×10^{-2}	4.0×10^{-6}	
cis-$[(bpy)_2Os(OH)_2]^{+/0}$	−0.55							
trans-$[(bpy)_2Os(OH)_2)_2]^{3+/2+}$	−0.01	6.3×10^{-9}	6.3×10^{-11}			3.2×10^{-1}	4.0×10^{-5}	
trans-$[(bpy)_2Os(OH)_2]^{+/0}$	−0.76							
$[(trpy)Os(OH_2)_3]^{3+/2+}$	−0.01	6.3×10^{-7}	1.0×10^{-8}	1.0×10^{-11}		6.3×10^{-3}	4.0×10^{-13}[d]	
$[(trpy)Os(OH)_3]^{0/-}$	−0.67							
$[(phen)Os(OH_2)_4]^{3+/2+}$	−0.33	2.0×10^{-9}	5.0×10^{-10}	3.2×10^{-11}	2×10^{-13}	4.0×10^{-3}	5.0×10^{-7}	4.0×10^{-18}[d]
$[(phen)Os(OH)_4]^{-/2-}$	−1.29							

[a] Aqua Os(III/II) redox potentials measured at pH 0 (μ = 1.0 M) and hydroxo Os(III/II) redox potentials measured at pH 13 (μ = 0.1 M). [b] Note ref in Table III. [c] Volts vs. SSCE at glassy-carbon electrodes. [d] Loss of two protons.

Table V. Acid Dissociation Constants for Higher Oxidation State Polypyridyl Complexes of Osmium at $\mu = 0.1$ M[a]

equilibrium	K_a	ref
$[(trpy)Os^{VI}(O)(OH)(OH_2)]^{3+} \rightleftharpoons [(trpy)Os^{VI}(O)_2(OH_2)]^{2+} + H^+$	3.4×10^{-3} [b] (6.3×10^{-3})	this work
$[(trpy)Os^{VI}(O)_2(OH_2)]^{2+} \rightleftharpoons [(trpy)Os^{VI}(O)_2(OH)]^{+} + H^+$	6.3×10^{-7}	this work
$[(phen)Os^{VI}(O)_2(OH_2)_2]^{2+} \rightleftharpoons [(phen)Os^{VI}(O)_2(OH)_2] + 2H^+$	2.2×10^{-13}	this work
cis-$[(bpy)_2Os^{V}(O)(OH)]^{2+} \rightleftharpoons [(bpy)_2Os^{V}(O)_2]^{+} + H^+$	6.3×10^{-6}	4a
$[(phen)Os^{IV}(O)(OH_2)_3]^{2+} \rightleftharpoons [(phen)Os^{IV}(O)(OH)_2(OH_2)] + 2H^+$	2.5×10^{-13}	this work

[a] K_a values estimated from the Pourbaix diagrams in Figures 3 and 4. [b] From spectrophotometric titrations.

same oxidation state and are complicated by the large spin–orbit coupling constant for Os, which imparts considerable allowedness to nominally "singlet to triplet" transitions.[19,20] Representative absorption spectra as a function of pH and probable band assignments are given elsewhere.[18]

Discussion

The availability of oxidation states VI–II for Os over a narrow potential range is a striking result of this and earlier work.[2,4] For example, for *cis*-$[(bpy)Os^{VI}(O)_2]^{2+}$ all of the oxidation states II–VI are observable within a potential range of 0.70 V at pH 4.0.[4] For $[(trpy)Os^{VI}(O)_2(OH_2)]^{2+}$ at pH 4.0, the potential difference between the Os(VI)/Os(III) and Os(III)/Os(II) couples is only 0.38 V, but the even more compressed potential range interrelating oxidation states VI and II is achieved at the expense of the intermediate oxidation states V and IV, which are unstable with respect to disproportionation. The appearance of so many oxidation states over a narrow potential range illustrates dramatically the ability of electron-donating oxo and hydroxo groups to stabilize higher oxidation states.

The appearance or nonappearance of stable intermediate oxidation states is a consequence of the closeness of the redox potentials interrelating the various oxidation states, differences in acid–base behavior between oxidation states, and electronic effects.[4a,21,22] For example, at pH >11, the $3e^-/3H^+$ trpy-based Os(VI)/Os(III) couple separates into a $1e^-$ Os(VI)/Os(V) couple and a $2e^-/2H^+$ Os(V)/Os(III) couple (Figures 2 and 4). The appearance of Os(V) as a stable oxidation state past pH 10 is a direct consequence of the difference in pH dependence between the $[(trpy)Os^{VI}(O)_2(OH)]^+/[(trpy)Os^{V}(O)_2(OH)]$ and $[(trpy)Os^{V}(O)_2(OH)]/[(trpy)Os^{III}(OH)_3]$ couples. As another example, in an earlier analysis it was concluded that electronic stabilization of Os(VI) by the *trans*-dioxo ligands plays an important role in leading to the overlap in potentials for couples between Os(VI) and Os(III).[4a]

When an oxidation state is "missing" and is within a multielectron couple, the measured potential of the multielectron couple is an average of the constituent couples. For example, past pH >11 where the Os(V)/Os(III) couple is observed, Os(IV) remains a missing oxidation state and is unstable with respect to disproportionation. This means that (1) $E°'$(Os(IV)/Os(III)) > $E°'$(Os(V)/Os(IV)), (2) Os(IV) is a stronger oxidant than Os(V), and (3) $E°'$(Os(V)/Os(III)) = [$E°'$(Os(IV)/Os(III)) + $E°'$(Os(V)/Os(IV))]/2. Where only one Os(VI)/Os(III) couple is observed, both Os(V) and Os(IV) are stronger oxidants than Os(VI). The patterns of thermodynamically stable oxidation states for a series of polypyridyl–aqua type complexes are summarized in Table III.

In explaining the Pourbaix diagrams for $[(trpy)Os^{VI}(O)_2](OH)]^+$ and $[(phen)Os^{VI}(O)_2(OH)_2]$, it was necessary to invoke

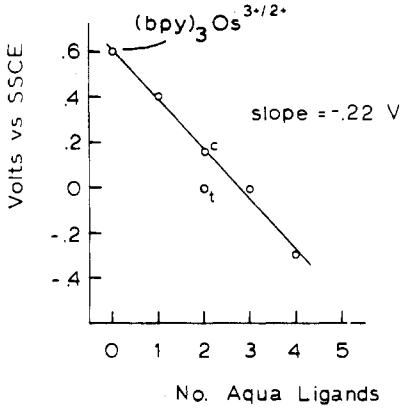

Figure 7. Plot of $E_{1/2}$(M(III)/M(II)) (volts vs. SSCE) vs. number of aqua ligands in the coordination sphere for the couples from $[M(bpy)_3]^{3+/2+}$ to $[M(bpy)(OH_2)_4]^{3+/2+}$. The cis and trans isomers of $[(bpy)_2M^{II}(OH_2)_2]^{2+}$ are represented by the letters c and t, respectively. $E_{1/2}$ values are from Table IV.

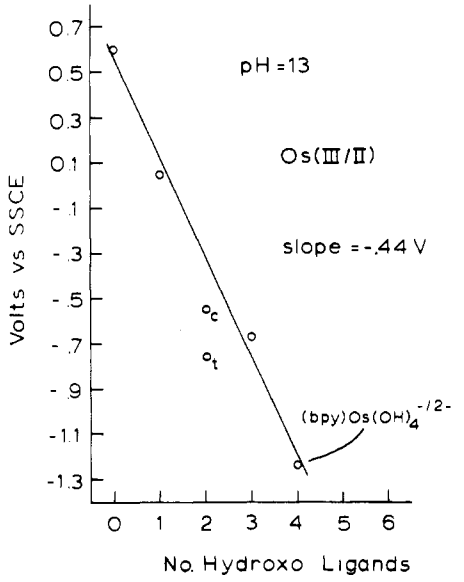

Figure 8. Plot of $E_{1/2}$(Os(III)/Os(II)) (V vs. SSCE) vs. the number of hydroxo ligands in the coordination sphere. The cis and trans isomers of $[(bpy)_2Os^{II}(OH)_2]$ are represented by the letters c and t, respectively. Potential values are from Table IV.

K_a values for processes involving the loss of two protons at a single pH or over a very narrow pH range as, for example, was invoked for $[(phen)Os(OH)_2(OH_2)_2]^+$ at pH ~8.7. As with a multielectron redox couple, a two-proton-loss process requires that K_a for the loss of the second proton must be greater or equal in magnitude to K_a for the loss of the first proton. The reported pK_a value is then an average of the two and the intermediate form a stronger acid than the initial form. On the basis of simple statistical and electrostatic arguments, the magnitude of the first K_a should exceed the second, and the intermediate acid, $[(phen)Os(OH)_3(OH_2)]°$, should be stable. The inversion in K_a values could arise, for example, by a special electronic stabilization factor appearing in the doubly deprotonated form, $[(phen)Os(OH)_4]^-$.

Acid Dissociation Constants. In Table IV are summarized pH-independent Os(III)/Os(II) reduction potentials and K_a values for Os(III) and Os(II) polypyridyl–aqua complexes. There are some subtle trends in the data, but the outstanding features are the greatly enhanced acidities at Os(III) and the loss of two protons at nearly the same pH value for $[(trpy)Os^{III}(OH)(OH_2)_2]^+$ and $[(phen)Os^{III}(OH)_2(OH_2)_2]^+$.

Acid dissociation constants for the higher oxidation state complexes are listed in Table V.

Trends in Redox Potentials. From the redox potential data now in hand it is possible to assess the role of ligand variations in

(19) Kober, E. M. Ph.D. Dissertation, University of North Carolina, Chapel Hill, North Carolina, 1982.
(20) Winkler, J. R.; Gray, H. B. *Inorg. Chem.* **1985**, *24*, 346.
(21) Gilbert, J. A.; Geselowitz, D.; Meyer, T. J. *J. Am. Chem. Soc.* **1986**, *108*, 1493.
(22) Geselowitz, D.; Kutner, W.; Meyer, T. J. *Inorg. Chem.* **1986**, *25*, 2015.

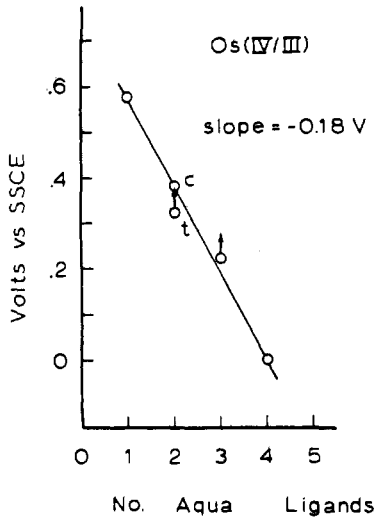

Figure 9. Plot of $E_{1/2}$(Os(IV)/Os(III)) (V vs. SSCE) at pH 4.5 for (1) $[(trpy)(bpy)Os^{IV}(O)]^{2+}/[(trpy)(bpy)Os^{III}(OH)]^{2+}$, (2) *cis*- and *trans*-$[(bpy)_2Os^{IV}(O)(OH_2)]^{2+}/[(bpy)_2Os^{III}(OH)(OH_2)]^{2+}$, and (4) $[(phen)Os^{IV}(O)(OH_2)_3]^{2+}/[(phen)Os^{III}(OH)(OH_2)_3]^{2+}$. The upward arrows indicate that only estimates of the lower limit for $E_{1/2}$ was obtained for these complexes. The letters c and t denote potentials for the cis and trans isomers of $[(bpy)_2Os^{IV}(O)(OH_2)]^{2+}$.

determining the relative magnitudes of redox potentials for the various couples observed. In Figure 7 are shown plots illustrating how potentials for the Os(III)/Os(II) couples vary as a pyridyl group is replaced by an aqua ligand for the series from $[Os(bpy)_3]^{3+/2+}$ to $[(bpy)Os(OH_2)_4]^{3+/2+}$, and in Figure 8 the same plot is shown where a pyridyl group is replaced by a hydroxo ligand. From the plots, replacing a pyridine by an aqua ligand decreases the oxidizing strength of Os(III) by –0.22 V and by a hydroxo group by –0.44 V. A number of factors determine such variations including differences in solvation energies and electronic effects arising from chemical bonding.[23] Important roles are, no doubt, played by the loss of stabilization of Os(II) by $d\pi-\pi^*$(py) back-bonding as pyridyl ligands are lost and, for hydroxo substitution, stabilization of Os(III) by enhanced $OH^-\rightarrow d\pi$(Os(III)) donation compared to $OH_2\rightarrow d\pi$(Os(III)) donation.

In Figure 9 are plotted $E_{1/2}$ values at pH 4.5 for the Os(IV)/Os(III) couples $[(trpy)(bpy)Os{=}O]^{2+}/[(trpy)(bpy)Os(OH)]^{2+}$, [*cis*- and *trans*-$(bpy)_2Os(O)(OH_2)]^{2+}/[(bpy)_2Os(OH)(OH_2)]^{2+}$, and $[(phen)Os(O)(OH_2)_3]^{2+}/[(phen)Os(OH)(OH_2)_3]^{2+}$. In the series of couples the $Os^{IV}{=}O^{2+}/Os^{III}{-}OH^{2+}$ groups are a constant feature with pyridyl groups successively replaced by aqua ligands. Replacement of a pyridyl group by an aqua ligand lowers the (IV)/(III) potential by –0.18 V and stabilizes Os(IV) but, interestingly, to a lesser degree than for Os(III). The difference in the response of the two couples to ligand variations begins to suggest how the potentials for the two types of couples can be manipulated by synthetic changes and, in particular, shows that the difference in potentials for the two couples is increased by electron-donating ligands and decreased by π-back-bonding ligands that stabilize Os(II).

There are insufficient data to make meaningful comparisons between Os(VI)/Os(V) couples. However, for the Os(VI)/Os(V) couples of *cis*- and *trans*-$[(bpy)_2Os^{VI}(O)_2]^{2+}$ and $[(trpy)Os^{VI}(O)_2(OH)]^+$ at pH >11 the Os(VI)/Os(V) couples are pH-independent. At pH >11 the difference in potentials, $\Delta E_{1/2} = E_{1/2}(trans\text{-}[(bpy)_2Os^{VI/V}(O)_2]^{2+/+}) - E_{1/2}([(trpy)Os^{VI/V}(O)_2(OH)]^{+/0}) = 0.31$ V, shows, once again, that the substitution of a pyridine ligand by a hydroxo group stabilizes the higher oxidation states and lowers reduction potentials.

Table VI. Reduction Potentials for Os(VI)/Os(III) and Os(VI)/Os(II) Couples as a Function of pH (V vs. SSCE)[a]

dominant form of Os(VI) in the couple at pH 7[b]	$E°'$(Os(VI)/Os(III)), V			$E°'$(Os(VI)/Os(II)), V		
	pH 0	pH 7	pH 14	pH 0	pH 7	pH 14
cis-$[(bpy)_2Os^{VI}(O)_2]^{2+}$[c]	0.77	0.40	0.13	0.62	0.24	–0.04
trans-$[(bpy)_2Os^{VI}(O)_2]^{2+}$[c]	0.60	0.23	–0.08	0.44	0.04	–0.25
$[(trpy)Os^{VI}(O)_2(OH)]^+$	0.51	0.06	–0.22	0.38	–0.06	–0.33
$[(phen)Os^{VI}(O)_2(OH)_2]$	0.43	–0.08	–0.45	0.24	–0.22	–0.62

[a] μ = 1.0 M at pH 0 or 14; μ = 0.1 M at pH 7. [b] Proton contents of the components of the couples vary with pH as in the Pourbaix diagrams in Figures 3 and 4 and in ref 4a. [c] Reference 4a.

Table VII. Reduction Potentials (V vs. SSCE)

couple	$E_{1/2}$, V	ref
Os(IV)/Os(III)		
$[(bpy)_3Os]^{4+/3+}$	2.8[a]	24
$[(trpy)(bpy)Os(Cl)]^{3+/2+}$	1.9[b]	25
$[(bpy)_2Os(Cl)_2]^{2+/+}$	1.6[b]	25
$[(trpy)(bpy)Os(O)]^{2+}/[(trpy)(bpy)Os(OH)]^{2+}$	0.55[c]	this work
cis-$[(bpy)_2Os(O)(OH_2)]^{2+}$/*cis*-$[(bpy)_2Os(OH)(OH_2)]^{2+}$	0.38[c]	4a
$[(phen)Os(O)(OH_2)_3^{2+}/[(phen)Os(OH)(OH_2)_3]^{2+}$	0.00[c]	this work
Os(V)/Os(IV)		
$[(trpy)(bpy)Os(O)]^{3+/2+}$	1.05[d]	26
Os(VI)/Os(V)		
trans-$[(bpy)_2Os(O)_2]^{2+/+}$	0.21[e]	4a
$[(trpy)Os(O)_2(OH)]^{+/0}$	–0.10[e]	this work

[a] In liquid SO_2 at Pt. [b] In CH_3CN at Pt. [c] In aqueous solutions at pH 4.5 with glassy-carbon electrodes. [d] $E_{p,a}$ value. [e] In aqueous solution at pH 11.0 with glassy-carbon electrodes.

An important feature of the redox chemistry of Ru and Os oxo complexes is their ability to function as multielectron-transfer oxidants,[7-10] and the complexes of interest here are feasibly three-electron Os(VI)/Os(III), or even four-electron, Os(VI)/Os(II), couples. Reduction potentials for the Os(VI)/Os(III) and Os(VI)/Os(II) couples at pH 0, 7, and 14 are collected in Table VI. There are a number of notable features in the data including the following: (1) As expected, the magnitudes of the potentials fall as pyridyl groups are replaced by O-based ligands. (2) Because of the significant pH and ligand dependences of the couples, they represent a series of potential multielectron oxidative or reductive couples having a wide range of potentials. (3) The couples involving $[(bpy)_2Os^{VI}(O)_2]^{2+}$ are considerably more strongly oxidizing for the cis isomer because of a significant stabilization of Os(VI) by the *trans*-dioxo group.[4a]

Role of the Oxo Ligand in Stabilizing High Oxidation States. In Table VII are collected reduction potentials for a series of couples that illustrate the special role that the *oxo* ligand plays in stabilizing higher oxidation states. For example, substitution of a pyridyl group by chloro or oxo ligands decreases the Os(IV)/Os(III) potential as shown by the potentials for the couples $[(bpy)_3Os]^{4+/3+}$ (2.8 V), $[(trpy)(bpy)Os(Cl)]^{3+/2+}$ (1.9 V), and $[(trpy)(bpy)Os(O)]^{2+}/[(trpy)(bpy)Os(OH)]^{2+}$ (0.55 V at pH 4.5). The ability of the oxo group to stabilize the higher oxidation state is dramatic and based on its abilities as a σ- and π electron donor and on its relative stability toward oxidation. Equally illustrative examples come from comparing the Os(V)/Os(IV) couple for $[(trpy)(bpy)Os(O)]^{3+/2+}$ ($E_{p,a}$ = 1.05 V) or the Os(VI)/Os(V) couples for *trans*-$[(bpy)_2Os(O)_2]^{2+/+}$ (0.21 V) or $[(trpy)Os(O)_2(OH)]^{+/0}$ (–0.10 V) with either the Os(IV)/Os(III) couples $[(bpy)_3Os]^{4+/3+}$ (2.8 V) or $[(trpy)(bpy)Os(Cl)]^{3+/2+}$ (1.9 V).

Acknowledgments are made to the National Science Foundation under Grant No. CHE-8304230 for support of this research.

Registry No. $[(trpy)Os(O)_2(OH)](NO_3)$, 104033-94-5; $K_2[Os(O)_2(OH)_4]$, 77347-87-6; $[(trpy)Os(O)(OH)(OH_2)]^{3+}$, 93255-64-2; [(trpy)-

(23) Buckingham, D. A.; Sargeson, A. M. *Chelating Agents and Metal Chelates*; Dwyer, F. P.; Mellor, D. P., Eds.; Academic: New York, 1964; Chapter 6.
(24) Gaudiello, J. G.; Bradley, P. G.; Norton, K. A.; Woodruff, W. H.; Bard, A. J. *Inorg. Chem.* **1984**, *23*, 3.
(25) Sullivan, B. P.; Meyer, T. J. *Inorg. Chem.* **1982**, *21*, 1037.
(26) Pipes, D. W.; Meyer, T. J. *Inorg. Chem.* **1984**, *23*, 2466.

$Os(OH_2)_3]^{3+}$, 93255-66-4; $[(trpy)Os(OH_2)_3]^{2+}$, 93255-67-5; $[(trpy)Os(O)_2(OH_2)]^{2+}$, 104033-95-6; $[(trpy)Os(OH_2)_2(OH)]^{2+}$, 104051-36-7; $[(trpy)Os(O)_2(OH)]^{+}$, 93255-65-3; $[(trpy)Os(OH)_2(OH_2)]^{+}$, 104033-96-7; $[(trpy)Os(OH)(OH_2)_2]^{+}$, 93255-69-7; $(trpy)Os(OH)_3$, 93255-68-6; $[(trpy)Os(OH)_3]^{-}$, 93279-99-3; $(trpy)Os(O)_2(OH)$, 93255-70-0; $[(phen)Os(O)_2(OH_2)_2]^{2+}$, 104033-97-8; $[(phen)Os(OH_2)_4]^{3+}$, 104033-98-9; $[(phen)Os(OH_2)_4]^{2+}$, 104033-99-0; $[(phen)Os(OH)(OH_2)_3]^{2+}$, 104034-00-6; $(phen)Os(O)(OH)_2(OH)$, 104034-01-7; $[(phen)Os(OH)_2(OH_2)_2]^{+}$, 104034-02-8; $(phen)Os(O)_2(OH)_2$, 69531-97-1; $[(phen)Os(OH)_3(OH_2)]^{-}$, 104034-03-9; $[(phen)Os(O)(OH_2)_3]^{2+}$, 104034-04-0; $[(trpy)(bpy)Os(O)]^{2+}$, 89463-60-5; $[(trpy)(bpy)Os(OH)]^{2+}$, 89463-59-2.

Notes

Contribution from the School of Chemical Sciences, University of Illinois, Urbana, Illinois 61801, and Department of Chemistry, University of Auckland, Auckland, New Zealand

Synthesis of Acetylene Adducts of an Iron–Molybdenum Cluster through Trapping Experiments on $(C_5H_5)_2Mo_2FeTe_2(CO)_x$: Conversion of *arachno*-$(C_5H_5)_2Mo_2FeTe_2(CO)_7$ to *closo*-$(C_5H_5)_2Mo_2FeTe_2(CO)_3(RC_2H)$

Leonard E. Bogan, Jr.,[†] George R. Clark,[‡] and Thomas B. Rauchfuss*[†]

Received March 11, 1986

In this note we describe an unusual substitution process for the recently prepared carbonyl cluster $Cp_2Mo_2FeTe_2(CO)_7$ (**1**), Cp = η^5-C_5H_5.[1] In our previous report we showed that the thermolysis of **1** in toluene solutions gives a number of Fe–Mo–Te-containing clusters in low yields. Importantly, when this thermolysis was conducted in the presence of $Fe(CO)_5$ or $CpCo(CO)_2$, good yields of Mo_2FeMTe_2 clusters (M = Fe or Co) were obtained, indicating that **1** is converted to a metastable intermediate that could be trapped with the added organometallic reagents. Labeling studies showed that the Cp_2Mo_2Fe portion of **1** remains intact throughout this cluster-building process. It is therefore very likely that the thermal activation of **1** simply involves decarbonylation; intermediates of the formula $Cp_2Mo_2FeTe_2(CO)_6$ or $Cp_2Mo_2FeTe_2(CO)_5$ would be formed in this way (eq 1). It is

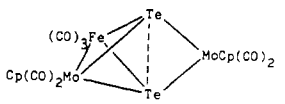

1

$$Cp_2Mo_2FeTe_2(CO)_7 \xrightarrow[\Delta]{-xCO} [Cp_2Mo_2FeTe_2(CO)_{7-x}] \xrightarrow{Fe(CO)_5} Cp_2Mo_2Fe_2Te_2(CO)_7 \quad (1)$$

interesting that the intermediate derived from **1** is unstable since it should be able to accommodate its coordinative unsaturation through the formation of additional metal–metal bonds resulting in nido or closo clusters. In this report we describe the results of our attempts to obtain further insight into this intermediate by trapping it with other reagents. These experiments provide an example where *four* carbon monoxide groups are displaced by a single ligand resulting in an iron–molybdenum–acetylene complex.[2]

Results and Discussion

Synthesis. We began this study by searching for ligands that would form adducts of the metastable intermediates thermally generated from **1**. When solutions of **1** were heated at 110 °C in the presence of H_2, N_2, azobenzene, or ethylene, the product distribution appeared to be independent of the substrate and only a small quantity of the products were soluble in organic solvents. However, when solutions of **1** were treated with certain acetylenes, we were able to isolate compounds of the formula $Cp_2Mo_2FeTe_2(CO)_3(C_2R_2)$ (**2** for R = H). Such compounds could be prepared with acetylene or phenylacetylene but not with diphenylacetylene (eq 2). In this regard the intermediate resembles

$$\underset{\mathbf{1}}{Cp_2Mo_2FeTe_2(CO)_7} + R_2C_2 \rightarrow \underset{\mathbf{2}\ (R = H)}{Cp_2Mo_2FeTe_2(CO)_3(R_2C_2)} + 4CO \quad (2)$$

$Cp_2Mo_2(CO)_4$, which reacts more readily with electron-rich acetylenes than with Ph_2C_2.[3]

The new compounds were obtained as black-green materials that are soluble in organic solvents, giving air-sensitive green solutions. They were formulated on the basis of microanalysis, mass spectrometry, and conventional spectroscopic data. The proton-coupled ^{13}C NMR spectrum of $Cp_2Mo_2FeTe_2(CO)_3(C_2H_2)$ showed that the acetylene moiety was intact since we observed both $|^1J(^{13}C,^1H)|$ (212 Hz) and $|^2J(^{13}C,^1H)|$ (8 Hz). The observed value for $^1J(C,H)$ is intermediate between that for C_2H_2 (249 Hz) and C_2H_4 (156 Hz) and is consistent with a dimetallatetrahedrane structure.[4] The ^1H NMR spectrum of $(MeCp)_2Mo_2FeTe_2(CO)_3(PhC_2H)$ provided further information on the symmetry of the molecule: the methyl groups are equivalent but the MeC_5H_4 signals appeared as several multiplets, indicating that the MeCp centroids do not lie on a symmetry plane in this derivative.

We have previously shown that ^{125}Te NMR was a sensitive probe for geometry of the M_3Te_2 core.[5] These previous measurements were however obtained only for nido or arachno clusters, as there existed no examples of closo M_3Te_2 clusters. The ^{125}Te chemical shift for **2** was found to be 931 ppm downfield with respect to Me_2Te. This shift is in the range found for the nido clusters. In contrast, δ_{Te} for **1** occurs at 1100 ppm *upfield* of the same standard.[1] This indicates that δ_{Te} for M_3Te_2 clusters is not directly influenced by the metal–metal bonding within the M_3 subunit. In fact the unusually high-field position of δ_{Te} for **1** may be a consequence of the magnetic anisotropy effects arising from the close Te···Te contact of 3.14 Å.[6]

The compound $Cp_2Mo_2FeTe_2(CO)_3C_2H_2$ was studied by cyclic voltammetry in THF solution and found to have two reduction waves at −1.27 (i_a/i_c = 1.02, ΔE_p = 92 mV) and at −1.89 V (i_a/i_c = 2.77, ΔE_p = 95 mV) vs. Ag/AgCl.

Structure of $(C_5H_5)_2Mo_2FeTe_2(CO)_3C_2H_2$ (2). In the lattice, the Mo_2FeTe_2 core is of approximate C_{2v} symmetry (Figures 1

[†] University of Illinois.
[‡] University of Auckland.

(1) Bogan, L. E., Jr.; Rauchfuss, T. B.; Rheingold, A. L. *J. Am. Chem. Soc.* **1985**, *107*, 3843.
(2) For a survey of acetylene complexes of metal clusters see: Sappa, E.; Tiripicchio, A.; Braunstein, P. *Chem. Rev.* **1983**, *83*, 203.
(3) Bailey, W. I., Jr.; Chisholm, M. H.; Cotton, F. A.; Rankel, L. A. *J. Am. Chem. Soc.* **1978**, *100*, 5764.
(4) Chisholm, M. H.; Folting, K.; Hoffman, D. M.; Huffman, J. C. *J. Am. Chem. Soc.* **1984**, *106*, 6794.
(5) Lesch, D. A.; Rauchfuss, T. B. *Inorg. Chem.* **1983**, *22*, 1854.
(6) For leading references for phosphido and μ_3-phosphinidine complexes and their ^{31}P NMR properties, see: Patel, V. D.; Cherkas, A. A.; Nucciarone, D.; Taylor, N. J.; Carty, A. J. *Organometallics* **1985**, *4*, 1792. Arif, A. M.; Cowley, A. H.; Pakulski, M.; Hursthouse, M. B.; Karauloz, A. *Organometallics* **1985**, *4*, 2227. Targos, T. S.; Geoffroy, G. L.; Rheingold, A. L. *Organometallics* **1986**, *5*, 12.

0020-1669/86/1325-4050$01.50/0